
This is an electronic reprint of the original article.
This reprint may differ from the original in pagination and typographic detail.

Mukherjee, Victor; Sokolov, Maksim; Pippuri-Mäkeläinen, Jenni; Hinkkanen, Marko;
Belahcen, Anouar
Comparative study of inner and outer rotor bearingless synchronous reluctance motors

Published in:
The Journal of Engineering

DOI:
[10.1049/joe.2018.8195](https://doi.org/10.1049/joe.2018.8195)

Published: 22/01/2019

Document Version
Publisher's PDF, also known as Version of record

Published under the following license:
CC BY

Please cite the original version:
Mukherjee, V., Sokolov, M., Pippuri-Mäkeläinen, J., Hinkkanen, M., & Belahcen, A. (2019). Comparative study of inner and outer rotor bearingless synchronous reluctance motors. *The Journal of Engineering*, 2019(17), 4375-4379. <https://doi.org/10.1049/joe.2018.8195>

This material is protected by copyright and other intellectual property rights, and duplication or sale of all or part of any of the repository collections is not permitted, except that material may be duplicated by you for your research use or educational purposes in electronic or print form. You must obtain permission for any other use. Electronic or print copies may not be offered, whether for sale or otherwise to anyone who is not an authorised user.

Comparative study of inner and outer rotor bearingless synchronous reluctance motors

eISSN 2051-3305
Received on 25th June 2018
Accepted on 30th July 2018
E-First on 26th April 2019
doi: 10.1049/joe.2018.8195
www.ietdl.org

Victor Mukherjee¹ ✉, Maxim Sokolov¹, Jenni Pippuri², Marko Hinkkanen¹, Anouar Belahcen^{1,3}

¹Department of Electrical Engineering and Automation, Aalto University, Finland

²VTT Technical Research Centre of Finland Ltd, Finland

³Department of Electrical Engineering, Tallinn University of Technology, Tallinn, Estonia

✉ E-mail: victor.mukherjee@aalto.fi

Abstract: In this study, the authors presented a systematic design procedure of outer rotor bearingless synchronous reluctance motor (SynRM). The proposed motor is compared with an already prototyped inner rotor bearingless SynRM at different operation points. It has been shown that a properly designed outer rotor SynRM can produce higher levitation forces than the inner rotor counterpart. The inner rotor motor produces higher torque and eccentric forces than the outer rotor motor.

1 Introduction

A bearingless synchronous reluctance motor (BSynRM) is an integration of the active magnetic bearing and a traditional synchronous reluctance motor in the same unit. An additional $p \pm 1$ pole pair winding is placed with the p -pole pair main winding in the stator slots. The interaction of the two windings generates an uneven distribution of the flux density in the airgap, which creates a magnetic force on the rotor [1]. Controlling the electromagnetic forces can cancel the gravity acting on the rotor and the shaft, and thus allowing the necessary levitation for the bearingless operation. This type of machine topology is beneficial in the high-speed applications [2] and in specific applications where the rotor and the stator cannot have any physical contact [3]. Depending upon the application requirement, the rotor can be placed inside the stator or outside it. An outer rotor topology, for traditional permanent magnet synchronous machines (PMSM), has already shown some added benefits in comparison to the inner rotor structure [4]. Due to the lower stator diameter, the outer rotor topology has less joule losses from the end winding than the inner rotor counterpart. Furthermore, the increased airgap diameter and permanent magnet surface in the outer rotor structure result in a higher airgap torque than in the inner rotor structure. However, designing an outer rotor reluctance motor is not straightforward as the torque is only a function of the reluctances difference of the d and q -axis of the rotor, which is also influenced by the airgap diameters and the flux barriers [5]. Nevertheless, designing a reluctance rotor for an SynRM is quite challenging, as the number of flux barriers and their width determine the electromagnetic performance of the motor [6, 7]. Moreover, there are very few researches on the outer rotor SynRM [8], as the topology is not so popular yet. In this work, a systematic design approach is presented, which can be used for designing an outer rotor normal and bearingless SynRM.

During the startup condition, the bearingless motors are eccentric in nature as they are resting on the safety bearing. Thus, the influence of the static eccentricity on the force production is quite critical. While lifting up the rotor, the force generated by the additional winding to compensate the eccentricity and to provide the acceleration of the rotor is a critical design criterion for a bearingless motor. The performance of the motors with different rotor topologies will show different behaviour under eccentricity, which will also influence the vibration of the motor. In [9], it is shown that the outer rotor bearingless PMSM has better performances in the starting characteristics. In addition, the ability to reach higher rotational speed of the outer rotor structure, due to the rotor being easy to reinforce without increasing the airgap and

without making compromises with the active area of the motor makes it an interesting choice for bearingless applications.

To the best knowledge of the authors, there is almost no literature on the design and performances of the outer rotor reluctance motor for the bearingless operation. The goal of this paper is to fill up the gap in the literature through a comparative analysis of the bearingless motor performance between an already prototyped inner rotor motor and a designed outer synchronous reluctance rotor, focusing primarily on the levitation force profile and the electromagnetic torque characteristics. Furthermore, different eccentricity cases are studied in detail to understand the levitation force characteristics of the motors. A brief mechanical stress analysis is also carried out to identify the feasibility of the motor at different speed ranges.

2 Methods of comparison

The performance of the machine is analysed using the finite element method with the magnetic vector potential formulation, which consists of solving the Ampere's law in the 2D cross-section of the machine. The equation to be solved is given as [10]

$$\nabla \times (\nu \nabla \times \mathbf{A}) = -\sigma \frac{\partial \mathbf{A}}{\partial t} - \sigma \nabla \Phi, \quad (1)$$

where \mathbf{A} is the magnetic vector potential and Φ is the reduced scalar potential. The reluctivity of the iron is considered as a non-linear function of the magnetic flux density. For computing the force, the Maxwell stress tensor method is used, where the stress tensor in the airgap is integrated over a line circle. In this paper, the line circle is selected at the 20% of the airgap from the rotor. Comsol Multiphysics 5.3a software package is used for the finite element calculation.

The machine windings are supplied with time varying sinusoidal current with a constant amplitude. The corresponding current density in the slots at a specific instant of time is shown in Fig. 1.

The machines' outer diameter and length are kept fixed for all the calculations. The parameters, which are unchanged for the comparisons for both the inner and outer rotor motors are given in Table 1.

2.1 Design choices of the outer rotor motor

The outer rotor motor for a PMSM is designed with an airgap diameter as selected from the following criteria [4]:

$$\Delta D = 2(h_d + h_{ys}) - 2h_{yr} \quad (2)$$

where ΔD is the changed airgap diameter, h_d , h_{ys} and h_{yr} are the height of the tooth, stator yoke and rotor yoke, respectively, of the inner rotor structure. However in a reluctance motor, the torque is only governed by the reluctance difference between the d - and q -axis of the rotor. Thus, selecting the airgap radius is not very straightforward, as the inductances are varied based on the rotor geometry and operation points, mainly due the saturation. The inner rotor geometry is already optimised by the selection of a proper flux barrier ratio of the rotor and a proper airgap radius, as widely used for inner rotor topology conventions [11]. For the outer rotor motor, different motors with different airgap radius are simulated, and the resulted torque is presented in Fig. 2 together with the levitation force.

The inner rotor motor has an airgap radius of 75 mm. According to (2), the outer rotor radius should be 78 mm. However, it can be seen from Fig. 2 that the airgap radius of 82 mm is the best design choice for a better torque and levitation force.

The k ratio for a reluctance motor is the ratio of the flux barrier to the iron part in the q -axis [12]. Next, different rotors were tested using different k -ratios. The torque results for the outer rotor with an airgap radius of 82 mm and the prototype inner rotor are presented in Fig. 3.

Although Fig. 3 shows that the highest torque is achieved for a k -ratio of 0.5, it has been observed during the simulations that the levitation and torque have different design compromises, which means that the maximum levitation force and the maximum torque do not necessarily occur at the same k -ratio. Finally, to compare the two topology, the outer rotor motor is designed with the airgap radius of 82 mm and the k -ratio of 0.5. To mitigate the spatial harmonics, some design suggestions from [13] have been used. The concept of rotor equivalent slot for a reluctance rotor is based on the equally divided rotor teeth along the airgap surface [14]. The rotor equivalent slot for the outer rotor has been kept to 14. The flux barriers for the inner and outer rotor has been manually further optimised to mitigate the spatial harmonics, and ensure a better mechanical stability.

2.2 Operational characteristics

The flux density of the inner rotor and outer rotor machines at rated torque and levitation are presented in Fig. 4. The motors are saturated more in the positive y -direction, which is the direction of levitation.

Both motors are supplied with the same rated main winding current and additional winding current with sinusoidal waveforms. The total simulated time is 0.1 s. The time stepping simulation is preceded by a stationary dc computation to mitigate the transient behaviour in the time-stepping simulations [15]. The torque, levitation force, and disturbance force (force in the x -direction) for the inner and outer rotor topology are shown in Fig. 5.

The levitation force occurs in the direction of the highest flux density, in this case along the positive y -axis with a strong force ripple. Additionally, due to the unsymmetrical distribution of the flux density in the non-levitating direction, a disturbance force ripple can be observed along the x -axis of the motor, although the time-average force is null. Furthermore, from Figs. 3 and 5, it is clear that the average torque of the inner rotor motor is higher than the torque of the outer rotor motor. However, the outer rotor motor has higher time-average levitation force. Furthermore, the torque and force ripples are lower in the case of outer rotor topology than in the case of inner rotor. These are interesting observations, which require more in-depth understanding. The magnetic flux densities and the harmonic analysis of it in the airgap of the two topologies are presented in Fig. 6; they correspond to operation point where the additional winding is not energised. It can be seen that the fundamental order of the flux density in the airgap of the inner rotor structure is slightly higher than the outer rotor structure.

This clearly explains that the torque for the inner rotor is higher than the outer rotor topology. The primary reason for a lower saliency ratio, and thereby lower torque for the outer rotor structure is the shape of the flux barriers. In the case of the outer rotor, the

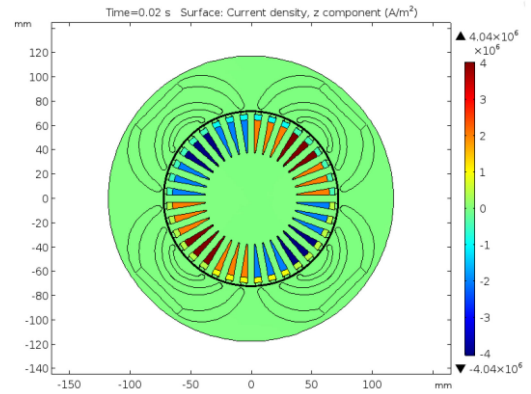


Fig. 1 Current density in the stator windings at a specific instant of time

Table 1 Design parameters, which are kept constant during the comparisons

Parameter	Value
rated current, main winding	31 A
no load current, main winding	22 A
rated current, additional winding	1 A
connection (main and additional windings)	Star
cated frequency (main and additional windings)	50 Hz
number of pole pairs (main winding)	2
number of pole pairs (additional winding)	1
outer diameter of the motor	235 mm
length of the motor	195 mm
number of slots	36
airgap length	1 mm
main winding slot area	91 mm ²
no of conductors (main winding)	16
additional winding slot area	26 mm ²
no of conductors (additional winding)	14

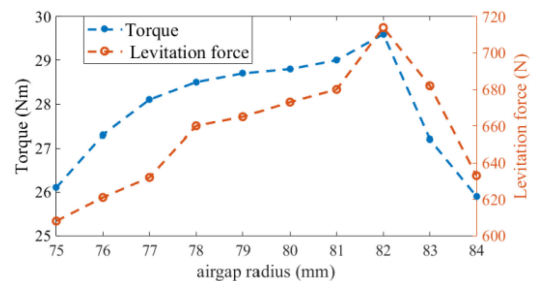


Fig. 2 Torque and levitation force averaged over one time-period as a function of the airgap radius for the outer rotor design

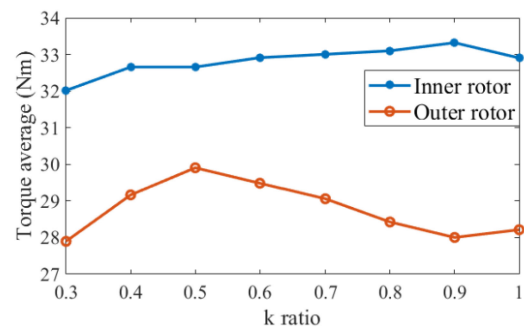


Fig. 3 Average torque of inner and outer rotor topology as a function of k -ratio

flux barriers are wider than in the case of inner rotor, which decreases the saliency ratio. Furthermore, the rotor in the outer rotor topology is slightly more saturated than the inner rotor

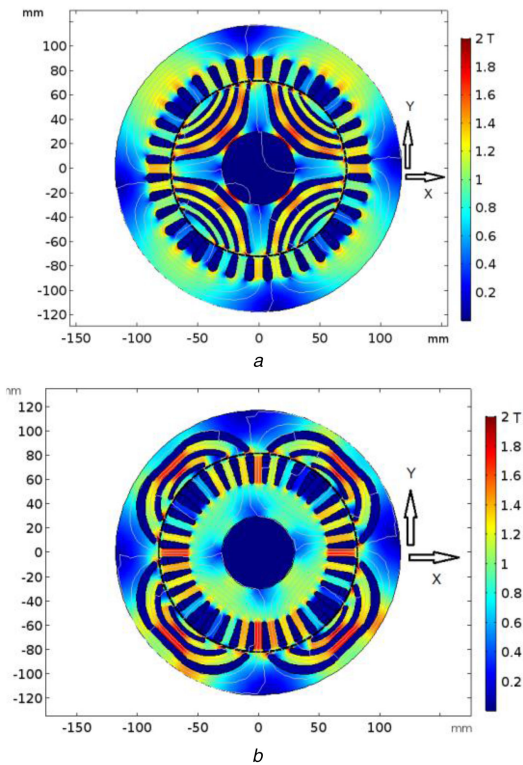


Fig. 4 Magnetic flux density of the motor
(a) Inner rotor, (b) Outer rotor at rated torque and levitation force at one time instant

counterpart, which also decreases the saliency ratios. Next, the magnetic flux density of the two topologies are presented in Fig. 7, where only the additional winding is supplied with a sinusoidal current of 3 A RMS and the main winding is disconnected. When the motor is supplied from the additional winding only, it operates without saturation. In this case, the higher airgap radius increases the inductances of the additional winding as the slots are exposed to a higher surface area of the rotor. The fundamental order of the magnetic flux density is then higher in the outer rotor motor than the inner rotor motor. Even when the motor is partially saturated, while the main winding is supplied, the magnetic flux density is slightly higher with the additional winding energised for the outer rotor motor than for the inner rotor motor topology. Next, the motor is operated at different speeds to understand the levitation force profile. It is the voltage and the mechanical stresses on the flux barriers that limit the speed. The levitation force at different speeds is shown in Fig. 8. Clearly, with higher speed, and limited voltage, the motor operates in the flux-weakening region which results in lower levitation force.

2.3 Eccentricity characteristics

When the rotor center axis shifts from the stator center axis, it creates an eccentric force, which is primarily the interaction of the $p \pm 1$ harmonics of the main windings with the fundamental harmonic [16]. When the relative position of the rotor center and the stator center is constant, it is called the static eccentricity, which is modelled in this work. When a bearingless motor is idle, its rotor rests on the safety bearings. While lifting up the rotor from its eccentric position to the center of the stator axis, a sufficient force needs to be generated to overcome the eccentric force, rotor weight and some necessary acceleration in the lifting up process. However, electromechanically there are different harmonics from the main winding and the additional winding which influence the process. The eccentric force is indeed governed by the magnetic flux density produced by the main winding, as the additional winding harmonics are too weak to influence. The levitation force, on the other hand, is governed mainly by the additional winding. The levitation force for the inner rotor topology and the outer rotor topology at different eccentricity levels and different additional winding current is shown in Fig. 9.

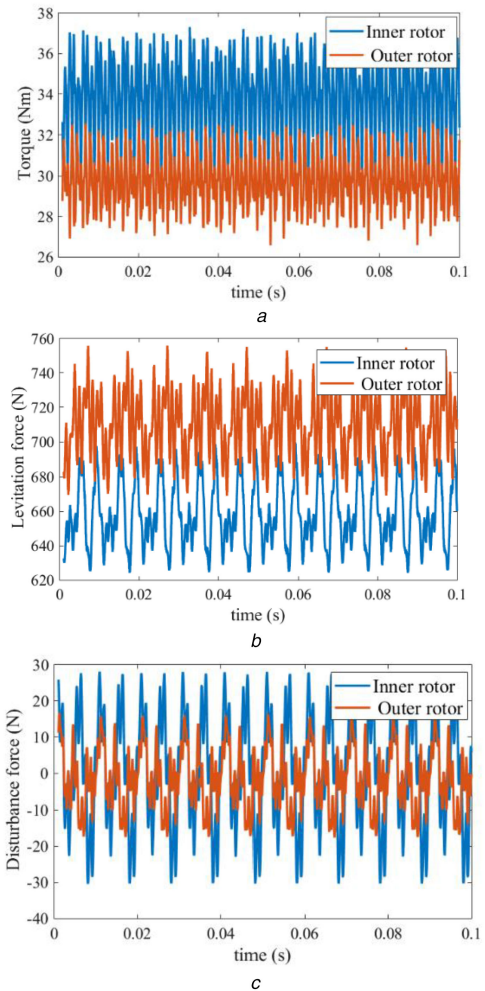


Fig. 5 Operational characteristics of the motors
(a) Torque, (b) Levitation force and, (c) Disturbance force for the inner and outer rotor topologies under rated operation

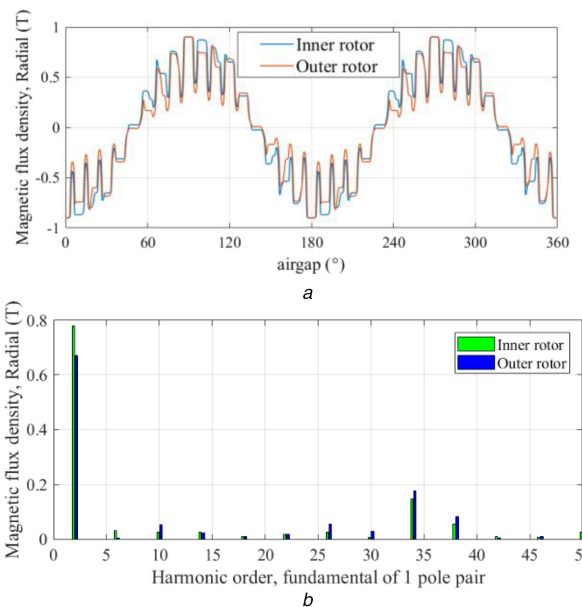


Fig. 6 Magnetic flux density characteristics of the inner and outer rotor motor while supplying only the main winding with sinusoidal current
(a) Magnetic flux density distribution in the airgap, (b) Fourier analysis of the magnetic flux density in the airgap

Since the magnetic flux density of the main winding for the outer rotor topology is lower than of the inner rotor topology, the eccentricity force produced in the outer rotor topology is also lower

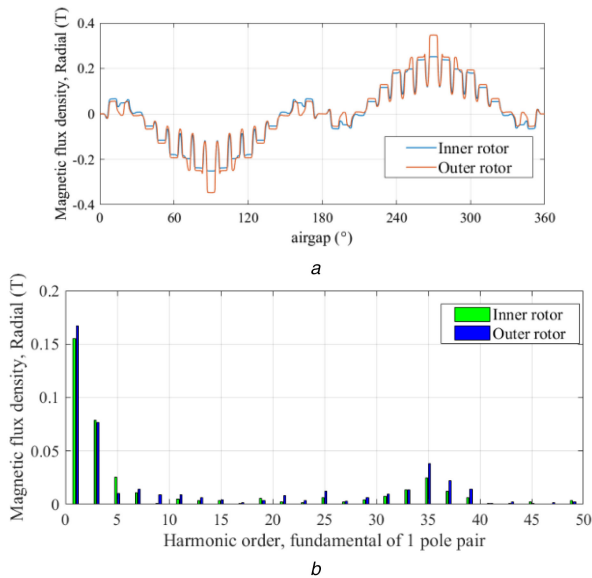


Fig. 7 Magnetic flux density characteristics of the inner and outer rotor motor while supplying only the additional winding with sinusoidal current (a) Magnetic flux density distribution in the airgap, (b) Fourier analysis of the magnetic flux density in the airgap

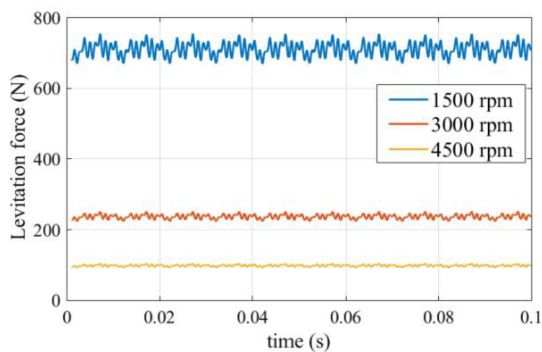


Fig. 8 Levitation forces for outer rotor motor at different speeds

than in the inner rotor motor. In addition, the higher magnetic flux density from the additional winding helps to generate a higher force in the levitation direction for the same additional winding current in the outer rotor motor. It can be concluded that in this case, the outer rotor motor has better rotor levitation characteristics than the inner rotor motor, which is again a crucial factor for designing a bearingless motor.

3 Mechanical stress

The speed of a radially laminated SynRM is often limited by the mechanical stresses in the flux barriers. Since the tip of the flux barrier has the maximum stress, it cannot be kept very close to the rotor outer surface. Again, keeping the tip too far from the rotor outer surface will hinder the saturation of the tip and thus the reluctance torque will decrease. Often, it is a design compromise of torque and mechanical stability for high-speed design. Since the motors in this work are primarily designed to operate at 1500 rpm, the flux barrier tip (or bridge) is placed only 1 mm from the rotor circumference. However, for high-speed application, this distance can be increased for a better mechanical stability by compromising the torque. The two motors are simulated at 5000 rpm and the von-Mises stress distribution is presented in Fig. 10.

The mechanical stress is slightly higher in the inner rotor structure than in the outer rotor one. The maximum von-Mises stress at any domain for different speeds is presented in Fig. 11.

It can be seen that the outer rotor structure has slightly better mechanical characteristics than the inner rotor structure. This is primarily due to the orientation of the flux barriers in the outer rotor structure, which are subjected to compressive stresses

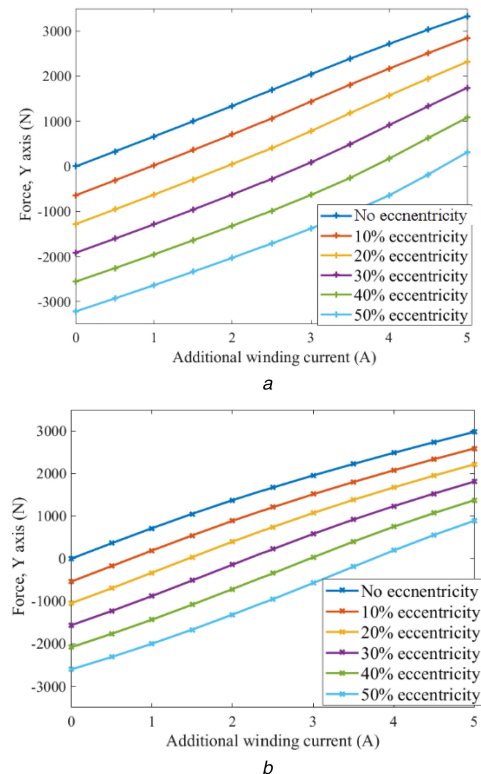


Fig. 9 Force in the levitation direction for (a) Inner rotor, (b) Outer rotor motor at different eccentricity levels and additional winding currents

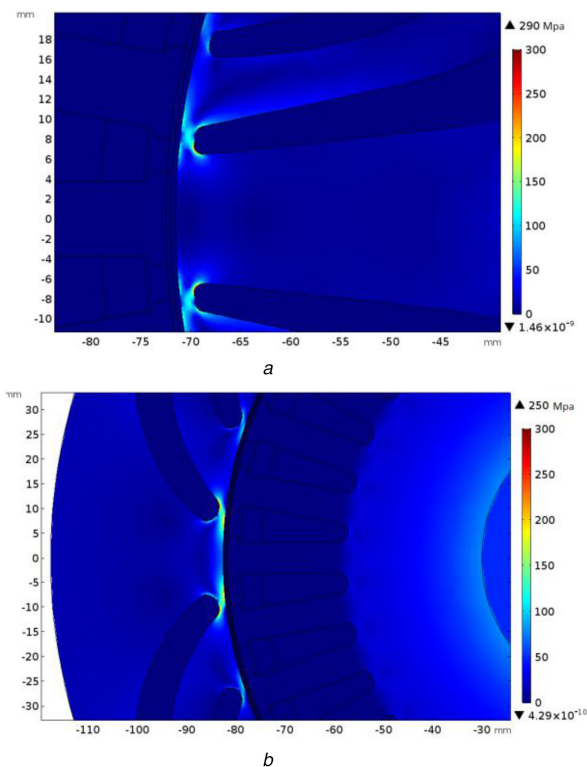


Fig. 10 von-Mises stress distribution of the (a) Inner rotor, and (b) Outer rotor motor

whereas those of the inner rotor structure are subjected to tensile stresses. The outer rotor structure can operate at more than 500 rpm higher speed than the inner structure for the same mechanical stress, especially in the high-speed region.

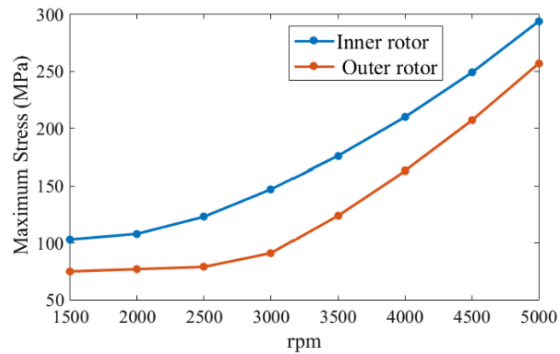


Fig. 11 Mechanical stress (von-Mises) for inner and outer rotor motor at different speeds

4 Conclusion

In this work, the inner and outer rotor configuration of the bearingless SynRM are compared on different operational characteristics. It has been found that the torque of a reluctance motor has a better profile in the inner rotor structure than in the outer rotor structure. A proper selection of the airgap radius is very critical for the outer rotor motor as the airgap radius is determined by several factors including the motor operation points and the saturation state of the motor, which influences the torque and the levitation force. A k -ratio of 0.5 has been found suitable for producing the maximum torque at the rated current. The levitation force profile of the properly designed outer rotor motor has shown better characteristics than that of the inner rotor motor. It has been found that the main winding of the inner rotor motor produces higher magnetic flux density in the airgap, and thus generate higher eccentricity forces on the rotor at standstill condition than the outer rotor motor. In addition, the additional winding for the outer rotor motor produces higher magnetic flux density in the airgap than the inner rotor motor. Moreover, it has been shown that mechanically, the outer rotor configuration has better stability than the inner rotor counterpart, which can be beneficial while operating the motor at higher speeds.

5 Acknowledgments

The authors acknowledge the Academy of Finland for financial support. This work was supported in part by the Estonian Research Council under the Grant number PUT1260.

6 References

[1] Takemoto, M., Yoshida, K., Itasaka, N., *et al.*: 'Synchronous reluctance type bearingless motors with multi-flux barriers'. 2007 Power Conversion Conf. – Nagoya, Nagoya, 2007, pp. 1559–1564
 [2] Schneider, T., Binder, A.: 'Design and evaluation of a 60,000 rpm permanent magnet bearingless high speed motor'. 2007 7th Int. Conf. on Power Electronics and Drive Systems, Bangkok, 2007, pp. 1–8

[3] Reichert, T., Nussbaumer, T., Kolar, J.W.: 'Bearingless 300 W pmsm for bioreactor mixing', *IEEE Trans. Ind. Electron.*, 2012, **59**, (3), pp. 1376–1388
 [4] Petrov, I.: 'Cost reduction of permanent magnet synchronous machines'. Ph.D. dissertation, Lappeenranta Univ. of Technology, Lappeenranta, Finland, 1987
 [5] Staton, D.A., Miller, T.J. E., Wood, S.E.: 'Maximising the saliency ratio of the synchronous reluctance motor', *IEEE Proc. B – Electric Power Applications*, 1993, **140**, (4), pp. 249–259
 [6] Howard, E., Kamper, M.J.: 'Weighted factor multiobjective design optimization of a reluctance synchronous machine', *IEEE Trans. Ind. Appl.*, 2016, **52**, (3), pp. 2269–2279
 [7] Ferrari, M., Bianchi, N., Doria, A., *et al.*: 'Design of synchronous reluctance motor for hybrid electric vehicles', *IEEE Trans. Ind. Appl.*, 2015, **51**, (4), pp. 3030–3040
 [8] Deshpande, Y., Toliyat, H.A.: 'Design of an outer rotor ferrite assisted synchronous reluctance machine (Fa- SynRM) for electric two wheeler application'. 2014 IEEE Energy Conversion Congress and Exposition (ECCE), Pittsburgh, PA, 2014, pp. 3147–3154
 [9] Yamada, T., Nakano, Y., Asama, J., *et al.*: 'Outer rotor consequent-pole bearingless motor with improved start-up characteristics', *IEEE Trans. Magn.*, 2008, **44**, (11), pp. 4273–4276
 [10] Arkkio, A.: 'Analysis of induction motors based on the numerical solution of the magnetic field and circuit equations'. Ph.D. dissertation, Helsinki Univ. of Technology, Espoo, Finland, 1987
 [11] Yammine, S., Henaux, C., Fadel, M., *et al.*: 'Synchronous reluctance machine flux barrier design based on the flux line patterns in a solid rotor'. 2014 Int. Conf. on Electrical Machines (ICEM), Berlin, 2014, pp. 297–302
 [12] Matsuo, T., Lipo, T.A.: 'Rotor design optimization of synchronous reluctance machine', *IEEE Trans. Energy Convers.*, 1994, **9**, (2), pp. 359–365
 [13] Pellegrino, G., Guglielmi, P., Vagati, A., *et al.*: 'Core losses and torque ripple in IPM machines: dedicated modeling and design tradeoff', *IEEE Trans. Ind. Appl.*, 2010, **46**, (6), pp. 2381–2391
 [14] Vagati, A., Pastorelli, M., Francheschini, G., *et al.*: 'Design of low-torque-ripple synchronous reluctance motors', *IEEE Trans. Ind. Appl.*, 1998, **34**, (4), pp. 758–765
 [15] Belahcen, A., Mukherjee, V., Far, M.F., *et al.*: 'Coupled field and space-vector equations of bearingless synchronous reluctance machine'. 2016 XXII Int. Conf. on Electrical Machines (ICEM), Lausanne, 2016, pp. 2581–2587
 [16] Tenhunen, A., Holopainen, T.P., Arkkio, A.: 'Effects of saturation on the forces in induction motors with whirling cage rotor', *IEEE Trans. Magn.*, 2004, **40**, (2), pp. 766–769